Characteristics of the Wind Field and Low-Level Jets in the Middle and Lower Troposphere over Chengdu, Southwest China

Tao Du *, Chen Wang, Xiaoyu Hu, Pengfei Tian, Yan Ren, Yunfan Song, Jiajing Du

Posted Date: 27 April 2026

doi: 10.20944/preprints202604.1861.v1

Keywords: wind field characteristics; Low-level jets; radar wind profiler; temporal variation; mountain-valley wind circulation

 doi:10.20944/preprints202604.1861.v1

Article

Characteristics of the Wind Field and Low-Level Jets in the Middle and Lower Troposphere over Chengdu, Southwest China

Tao Du [1,2,*], Chen Wang [3], Xiaoyu Hu [4], Pengfei Tian [3], Yan Ren [5], Yunfan Song [1,2] and Jiajing Du [1,2]

[1] Heavy Rain and Drought-Flood Disasters in Plateau and Basin Key Laboratory of Sichuan Province, Institute of Tibetan Plateau Meteorology, China Meteorological Administration, Chengdu, 610072, China
[2] Institute of Plateau Meteorology, Chinese Academy of Meteorological Sciences, Beijing, 100081, China
[3] College of Atmospheric Sciences, Lanzhou University, Lanzhou, 730000, China
[4] Chongqing Research Institute of Big Data, Peking University, Chongqing, China
[5] Collaborative Innovation Center for Western Ecological Safety, Lanzhou University, Lanzhou 730000, China
* Correspondence: dutao@cma.gov.cn

Highlights

What are the main findings?

- Validation of RWP performance over the western Sichuan Basin. the wind profiler radar achieves an annual effective detection height of 7.4 km with good consistency against radiosonde data.
- High-resolution vertical wind structure over the Chengdu basin based on one-year RWP observations. horizontal wind speed accelerates above 3 km (strongest in winter), and low-level winds shift from mountain-valley breezes to westerly control aloft.
- The spatiotemporal evolution of low-level jets over the Chengdu basin is characterized. LLJ occurrence peaks in July (followed by April), jet core heights are 0.9-1.5 km, and both frequency and intensity are higher at night.

What are the implications of the main findings?

- These findings deepen our understanding of boundary layer structure and wind field evolution over complex basin terrain, providing a high-resolution observational basis for model improvements.
- The results offer scientific support for the early warning of heavy rainfall events, the management of air pollution, and the safe operation of the low-altitude economy.
- The detailed characterization of LLJ spatiotemporal variability serves as a valuable reference for wind energy development, aviation safety, and studies of heat, moisture, and pollutant transport in the lower atmosphere.

Abstract

Low-level jets (LLJs) play an important role in the transport of heat, water vapor, and pollutants. Based on one year of tropospheric wind profiler radar (RWP) observations, this study systematically analyzes the wind field structure in the middle and lower troposphere over the Chengdu region, as well as the vertical distribution and evolution characteristics of LLJs. The results show that the effective detection height of the wind profiler radar reaches 7.4 km throughout the year, demonstrating good consistency with radiosonde data. Horizontal wind speed accelerates significantly above 3 km, with the highest vertical gradient of wind speed occurring in winter. The prevailing wind direction in the lower layer is mainly influenced by mountain-valley breezes; with increasing altitude, the westerly belt gradually becomes the dominant wind system. Within the atmospheric boundary layer (below 1 km), the wind field exhibits a distinct diurnal variation: easterly winds dominate in the afternoon, shifting to northerly winds at night. The peak surface wind speed

 doi:10.20944/preprints202604.1861.v1

occurs in the afternoon, while the peak upper-level wind speed occurs at night. The occurrence frequency of LLJs is highest in July, followed by April. The prevailing wind directions of LLJs are north-northeasterly and northeasterly, and the jet core heights are mainly distributed between 0.7 and 1.9 km. Both the occurrence frequency and intensity of LLJs are higher at night than during the day. These findings deepen our understanding of the boundary layer structure over complex basin terrain.

Keywords: wind field characteristics; Low-level jets; radar wind profiler; temporal variation; mountain-valley wind circulation

1. Introduction

Observations of atmospheric wind profiles are critical for predicting extreme rainfall events, forecasting tropical cyclones and hurricanes, understanding persistent haze pollution episodes, and investigating complex aerosol–cloud–precipitation interactions [1–6]. Low-level jets (LLJs) are an important weather phenomenon with notable impacts globally [7–12]. The strong wind shear associated with LLJs can induce intermittent turbulence near the surface and modulate the transport of surface heat, moisture, and pollutants. As a result, LLJs play a key role in pollutant dispersion, the urban heat island effect, wind energy development, aviation safety, and heavy precipitation processes [13–16]. The formation of LLJs arises from the combined effects of multiple mechanisms, including inertial oscillation, topographic thermal forcing, and synoptic-scale forcing [17–22].

The characteristics of wind fields in the middle and lower troposphere are governed by a range of factors, including atmospheric dynamics, thermal conditions, topography, underlying surface properties, and anthropogenic influences [23–25]. In recent years, numerous studies have employed diverse datasets to investigate tropospheric wind fields across different regions worldwide [26–30]. For instance, Yan (2021) [30] identified six regions in China with high frequency LLJs using long-term radiosonde observations. Zheng (2024) [23] employed Doppler wind lidar to reveal that the dominant near-surface wind direction in the lower troposphere over Xining is primarily influenced by valley-mountain circulation. Radar wind profiler (RWP), which operate based on the scattering of electromagnetic waves by atmospheric turbulence, enable real-time, continuous monitoring of three-dimensional wind field information in the upper atmosphere [31–33]. Offering considerable advantages over conventional ground-based in situ or remote sensing observations, wind profiler measurements have been successfully applied in various contexts, including air quality studies and weather forecasting [34–40]. For example, Wei (2014) [39] conducted a comparative analysis of LLJ characteristics in Tianjin and Shanghai using RWP data, revealing that nighttime LLJs are significantly stronger and more frequent than daytime occurrences. Similarly, Miao (2018) [40] systematically investigated LLJ characteristics in Beijing and Guangzhou using RWP observations. Yang (2024) [41] performed statistical analyses of the vertical distribution of wind fields and wind shear characteristics based on RWP data. Li (2026) [42] revealed the nationwide variability of LLJs prior to warm-season nocturnal rainfall in China by RWP.

Chengdu is located in the western part of the Sichuan Basin. It features complex topography, bordering the eastern margin of the Qinghai-Tibet Plateau to the west and the Longquan Mountains to the east, and has a distinctive climate. Moreover, Chengdu has a permanent resident population of over 21 million and a relatively high population density. The wind field structure in the middle and lower troposphere over this region, particularly the LLJ, plays a critical role in the occurrence of local hazardous events, including persistent heavy rainfall, haze pollution, and low-level wind shear. Existing studies on the Chengdu area have primarily focused on the characteristics of the low-level wind field and its relationships with heavy precipitation or pollution processes [43–48], however, systematic research on the three-dimensional wind field and LLJ features in the middle and lower troposphere remains lacking.

 doi:10.20944/preprints202604.1861.v1

This study utilizes one year of high spatiotemporal resolution RWP observation data from a representative site in the Chengdu region (the Wenjiang Meteorological Observation Base). It systematically investigates the vertical distribution and evolution characteristics of the wind field and LLJs in the middle and lower troposphere, aiming to provide support for local meteorological operations, related scientific research, and low-altitude meteorological applications. The structure of this paper is as follows: Section 2 introduces the study area, observation instruments, data, and methods. Section 3 provides a detailed analysis of the wind field in the middle and lower troposphere over the Chengdu region, as well as the vertical distribution and evolution characteristics of LLJs. Section 4 presents the discussion. Section 5 summarizes the main conclusions.

2. Materials and Methods

2.1. Observation Site, Instrument, and Measurement

This study utilizes one year of observational data (from September 1, 2023 to August 31, 2024) collected at the meteorological observation base in Wenjiang District, Chengdu (103.861°E, 30.749°N, 548.9m above sea level), including balloon soundings, RWP observations and surface wind direction and speed data. The site topography and RWP equipment are shown in Figure 1. The sounding and RWP observations are located approximately 50 m apart. The RWP instrument is a TWP8-L tropospheric wind profile radar, developed by Beijing Minstar Radar Co., Ltd., China, with technical parameters listed in Table 1. Its observational capabilities include the retrieval of horizontal wind direction, wind speed, and vertical velocity across 42 height layers within approximately 8 km. The vertical resolution is 120 m below 2 km and 240 m above 2 km. The RWP provides three temporal resolution data products: 6-minute real-time data, 30-minute averaged data, and 1-hour averaged data [34]. Because real-time minute-scale data contain transient atmospheric fluctuations [39,49], the wind data analyzed in this study are hourly averaged observations that have passed the manufacturer's 100% confidence test. To investigate seasonal differences in atmospheric wind field characteristics, the data are divided into four seasons: spring (March-May, MMA), summer (June-August, JJA), autumn (September-November, SON), and winter (December-February, DJF).

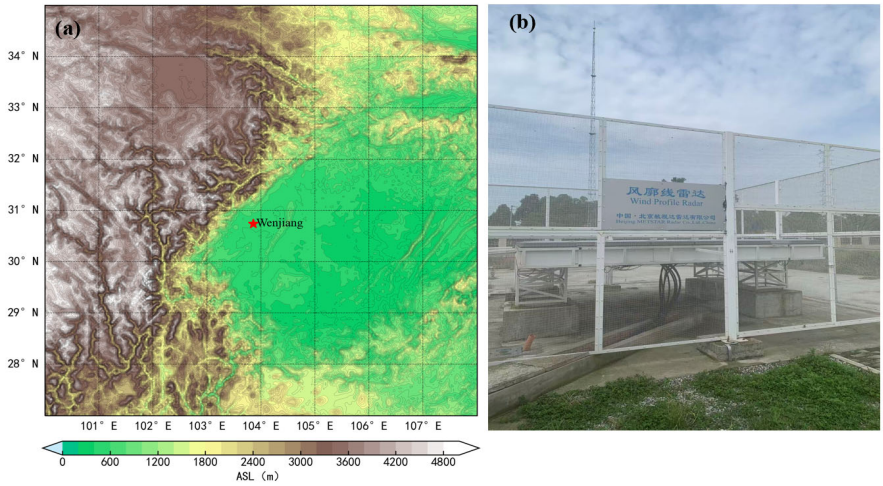

Figure 1. (a) Terrain of the Chengdu Wenjiang Meteorological Observation Base and **(b)** RWP.

Table 1. Main Technical Parameters of the TWP8-L Wind Profiling Radar System.

parameters	Technical Performance Indicators
Radar System	Fully Coherent Pulse Doppler System
Operating Frequency	1290MHz

 doi:10.20944/preprints202604.1861.v1

Maximum Detection Altitude	≥3km
Minimum Detection Altitude	≤100m
Measurement Performance	Wind Speed Measurement Range: 0–60 m/s; Wind Direction Measurement Range: 0–360°

2.2. Radar Wind Profiler Data Quality Control

The quality control of wind profiler measurements was rigorously conducted following the procedures proposed by Wei (2014) [39]. First, the wind profiles at each time were checked, and a profile was discarded if more than 40% of the data points were outliers or missing. Next, We then removed significant outliers whose variances within a given time period or height range differed from the mean by more than 2.5 standard deviations. Finally, discontinuous or missing values were estimated by linear interpolation. After quality control, a total of 8431 valid hourly wind profile datasets were obtained for the Wenjiang station.

2.3. Definition of LLJ

On the basis of the LLJ strength (i.e., wind maximum at the jet nose) and the decrease in speed above the jet nose [12,39,40], the LLJs are subjectively classified into four categories. Jets in the LLJ-1 category have a maximum wind speed greater than or equal to 10 m/s in the lowest 3 km above the ground level (AGL), and the decrease of wind speed above the jet but below 3 km must be at least 5 m/s. The LLJ-2 through LLJ-4 criteria are similar, except that the maximum speed criteria are 12, 16, and 20 m/s, and the falloff criteria are 6, 8, and 10 m/s. Note that these LLJ categories are inclusive. For example, the LLJ-1 category includes other stronger jet categories (i.e., LLJ-2, LLJ-3, and LLJ-4). In addition to the above mentioned wind speed criteria, the continuous evolution of LLJ is also considered in this study. As a sanity check, the wind profiles of the previous hour and the next hour are examined, and only those profiles with jet noses persisting for more than 2 hours are considered as a LLJ event.

3. Results

In this section, the detection performance of the RWP is first evaluated. Based on this, the characteristics of the wind field and LLJs at this site are systematically investigated, with a focus on the vertical distribution, seasonal variation, and diurnal variation of horizontal wind, vertical wind, and LLJs of different intensities.

3.1. Radar Wind Profiler Performance Evaluation

The performance of the RWP itself, precipitation, spatial inhomogeneity of wind, and ground clutter can all affect the quality of RWP observations. To better understand and utilize RWP wind field data, it is necessary to evaluate and analyze the performance of the RWP [41]. The three system performance indicators for radar performance evaluation include data acquisition rate (DAR), effective detection height, and data confidence[34]. The DAR is calculated as the ratio of data passing the confidence test to the total expected data at each altitude level [34]. Altitudes with a DAR above 0.8 are considered effective detection heights. To quantitatively evaluate the wind measurement capability of the RWP, the monthly and diurnal variations of the DAR were statistically analyzed (Figure 2). The data for all 12 months of the year show that the DAR exceeds 80% below the altitude of 7.4 km, with the effective detection height reaching up to 8 km in some months. Therefore, the effective detection height of the radar can be determined as 7.4 km, beyond which the DAR decreases rapidly with increasing altitude. The DAR from May to August were lower than in other months, with the highest annual rate observed in October (98.7%) and the lowest in August (90.1%). Differences in atmospheric temperature, humidity conditions, and turbulence intensity are likely responsible for the monthly variations in the DAR. A noticeable "inflection" phenomenon occurs near

 doi:10.20944/preprints202604.1861.v1

3.1 km, which is attributed to the radar pulse emission switching from low mode to high mode at this altitude, the abrupt change in signal-to-noise ratio results in a discontinuity in the DAR. As shown in the diurnal variation characteristics of the DAR (Figure 2b), the DAR exhibits a unimodal distribution, peaking at 22:00 and reaching its lowest point at 13:00.

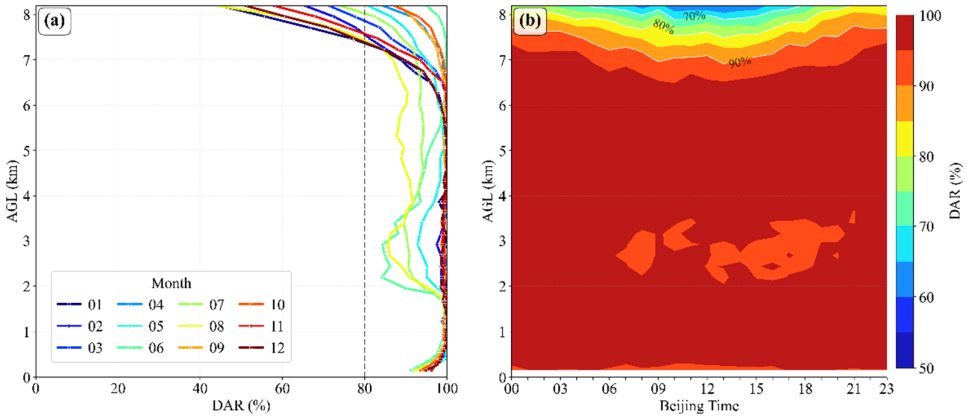

Figure 2. (a) Monthly data acquisition rate and **(b)** diurnal variation of data acquisition rate for the RWP.

To further evaluate the data quality of the RWP, a comparative verification was conducted between RWP data and synchronous balloon radiosonde observations. Balloon soundings are conducted twice daily (08:00 and 20:00). Due to differences in detection principles and observation times between the RWP and balloon soundings, RWP horizontal wind data adjacent to the balloon sounding observation times were selected. The nearest-neighbor interpolation method was applied to interpolate the radiosonde-observed horizontal winds to the corresponding heights of the RWP to mitigate the impact of spatial and temporal mismatches. Subsequently, the wind speed differences between the RWP and radiosonde data were calculated (Figure 3).

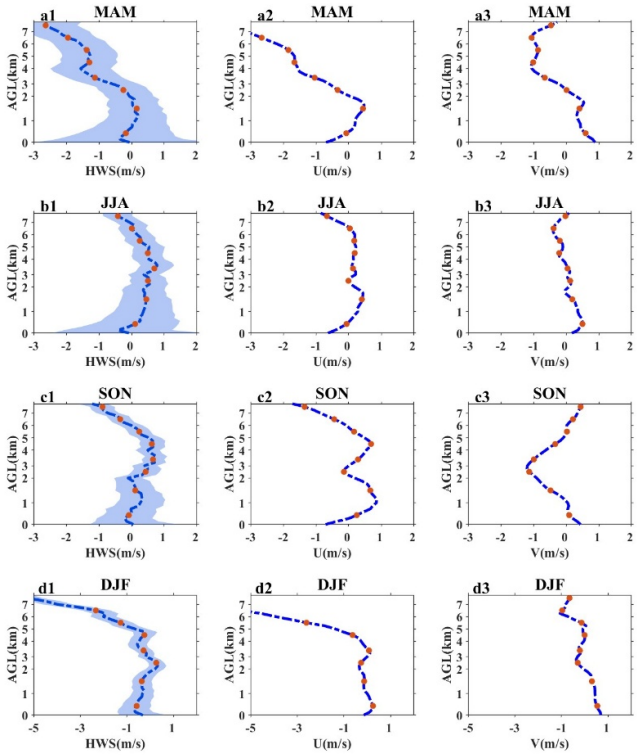

 doi:10.20944/preprints202604.1861.v1

Figure 3. Vertical distribution of mean errors in horizontal wind speed **(a1-d1)**, zonal wind **(a2-d2)**, and meridional wind **(a3-d3)** between radiosonde and RWP data across four seasons in Chengdu Wenjiang (blue curves represent mean errors, dark blue shading denotes root mean square errors, and red dots indicate mean errors at each kilometer altitude).

Comparing the vertical distribution of mean errors in horizontal wind speed (HWS) across different seasons (Figure 3(a1-d1)), the mean errors in summer and autumn are relatively small (±1 m s^{-1}) at all altitudes. In spring and winter, the mean errors are smaller below 4 km and 6 km, respectively, after which they increase rapidly with altitude. The variation of mean errors in zonal wind (U-wind) with height across seasons is similar to that of horizontal wind speed (Figure 3(a2-d2)). The mean errors in meridional wind (V-wind) are generally smaller than those in U-wind, Consistent with the research findings of other scholars[49,50]. with the smallest errors observed in summer (Figure 3(a3-d3)), indicating that the consistency between the two observations is best in summer. Although there are certain discrepancies, the RWP data are generally in good agreement with the radiosonde observations in the middle and lower troposphere (0-6 km).

3.2. Vertical Distribution Characteristics of the Atmospheric Wind Field

Statistical analysis was conducted on the vertical distribution characteristics of horizontal wind speed and direction from RWP data (Figure 4). The prevailing wind direction is defined as the azimuth with the highest frequency of occurrence. The variations in mean wind profiles across seasons are shown in Figure 4a. The mean wind speed throughout the atmospheric column is highest in winter (8.0 m/s), followed by spring (7.3 m/s) and autumn (6.8 m/s), with the lowest mean wind speed occurring in summer (5.9 m/s). The mean wind speed increases with altitude in all seasons, with the greatest rate of increase observed in winter, rising from 2.0 m/s at the lowest level to 21.4 m/s at the highest level. In contrast, the wind speed increases most slowly in summer, rising from 3.3 m/s at the lowest level to 16.1 m/s at the highest level. Below 3 km, wind speeds are lowest in winter and highest in summer. Above 3 km, winter wind speeds gradually become the highest, while summer wind speeds become the lowest.

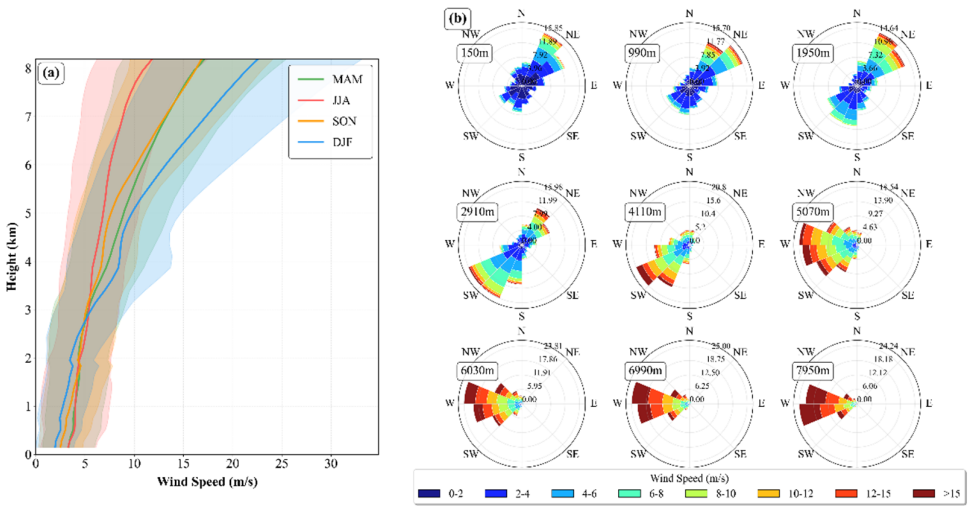

Figure 4. (a) Mean wind profiles across four seasons (shaded areas represent standard deviations), and **(b)** wind speed and direction rose diagrams at different altitudes.

Figure 4b presents the annual mean wind speed and direction rose diagrams for nine typical altitude levels (150 m, 990 m, 1950 m, 2910 m, 4110 m, 5070 m, 6030 m, 6990 m, and 7950 m). In the lower layer (below 2 km), the mean wind direction exhibits high variability, with the prevailing wind direction being northeasterly. Wind speeds are relatively low and increase slowly with height, with the mean wind speed rising from 2.7 m/s at 150 m to 4.1 m/s at 1950 m. In the middle layer (2-5 km),

 doi:10.20944/preprints202604.1861.v1

the prevailing wind direction shifts to southwesterly, and wind speeds increase with altitude, with the mean wind speed rising from 4.1 m/s at 1950 m to 8.4 m/s at 5070 m. In the upper layer (5-8 km), the prevailing wind direction is westerly, consistent with classical geostrophic wind theory. Wind speeds increase significantly with height, with the mean wind speed rising rapidly from 8.4 m/s at 5070 m to 15.8 m/s at 7950 m.

Further analysis was conducted on the probability distributions of horizontal wind direction (HWD), horizontal wind speed (HWS), and vertical wind speed (VWS) with height (Figure 5). The vertical distribution characteristics of prevailing wind direction show slight variations across seasons (Figure 5(a1-a4)). In the lower layer (below 2 km), the prevailing wind directions are north-northeasterly and northeasterly. The dominant wind direction shifts from north-northeasterly in the lower boundary layer to northeasterly, which is largely consistent with the low-altitude wind field distribution observed at the Dayi station[48]. This phenomenon may be attributed to the blocking effects of the plateau and mountainous terrain, as well as the unique topography of the Sichuan Basin. Among the seasons, spring and winter exhibit a higher proportion of northeasterly winds, while summer and autumn have a higher proportion of north-northeasterly winds. In the middle layer (2-5 km), the prevailing wind directions are southerly and southwesterly, with the frequency distribution of wind directions tilting from southerly to southwesterly as altitude increases. In the upper layer (5-8 km), the prevailing wind direction is westerly, with the lowest proportion of prevailing westerly winds occurring in summer and the highest in winter. From summer to winter, the altitude of prevailing westerly winds decreases from 6 km to 5 km.

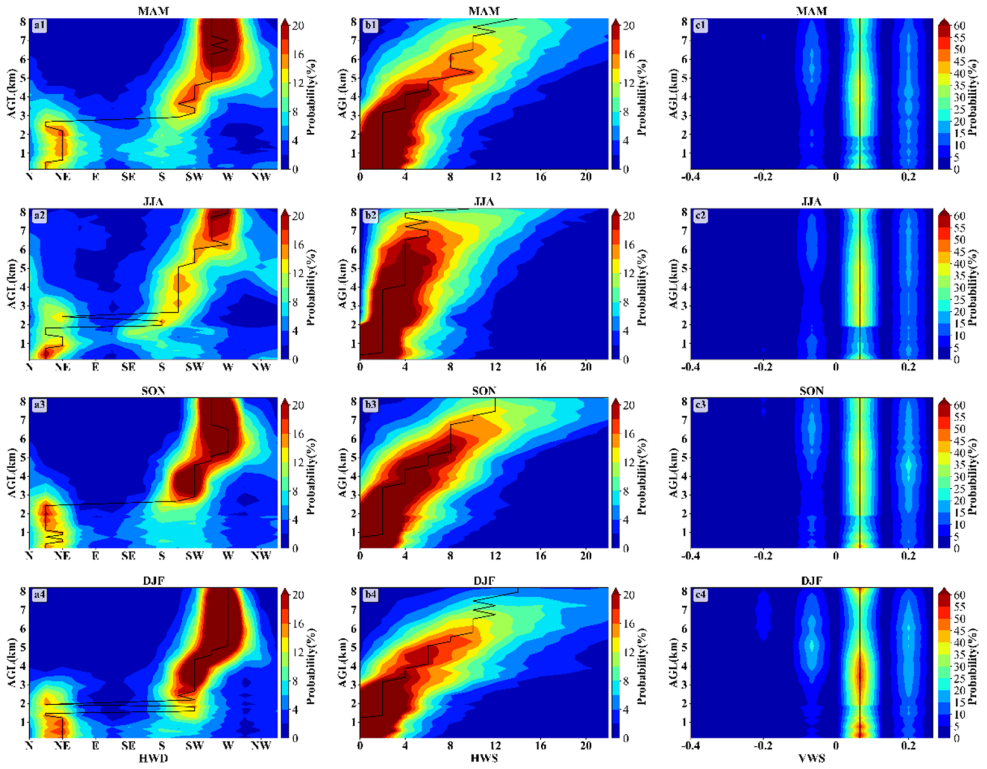

Figure 5. Probability distributions of horizontal wind direction (HWD, **a1-a4**), horizontal wind speed (HWS, **b1-b4**), and vertical wind speed (VWS, **c1-c4**) at different altitude levels across the four seasons. The subplots from the first to the fourth rows represent spring, summer, autumn, and winter, respectively, with solid lines indicating mean values.

In all four seasons, HWS increases slowly with height below 3 km and accelerates rapidly above 3 km (Figure 5(b1-b4)), similar to the frequency distribution of horizontal wind speed in Hefei [25]. Moreover, the HWS in cold seasons is generally higher than in warm seasons, particularly in winter,

 doi:10.20944/preprints202604.1861.v1

when the HWS in the upper atmosphere can reach a maximum compared to other seasons. This may be attributed to the fact that the upper-level high-speed winds from the westerlies exhibit their maximum volume vertically from 500 hPa to 100 hPa during winter [51]. The HWS in the lower atmosphere is more concentrated than in the upper layers, Consistent with the research findings of other scholars [23,25].

Regarding the vertical wind speed observed by the RWP, downward vertical velocity is defined as positive, and upward vertical velocity as negative [48]. The main distribution range of VWS is -0.2 to 0.2 m/s (Figure 5(c1-c4)), with the high-frequency center concentrated around 0.05 m/s, indicating the dominance of downdrafts. The high-frequency center is more concentrated in winter.

3.3. Diurnal Variation Characteristics of Atmospheric Wind Fields

The near-surface wind direction and speed in each season exhibit pronounced diurnal variations (Figure 6). The diurnal variation curves of near-surface wind speed show a unimodal pattern, with the peak wind speed occurring at 14:00 in all seasons, while the trough occurs before sunrise. Specifically, the trough appears at 07:00 in spring and autumn, at 06:00 in summer, and at 09:00 in winter. The peak near-surface wind speed is highest in spring, followed by summer, and lower in autumn and winter. Influenced by the mountain-valley breeze circulation, the prevailing near-surface wind direction is easterly (valley breeze) during the daytime afternoon (12:00-17:00) and northerly (mountain breeze) at night.

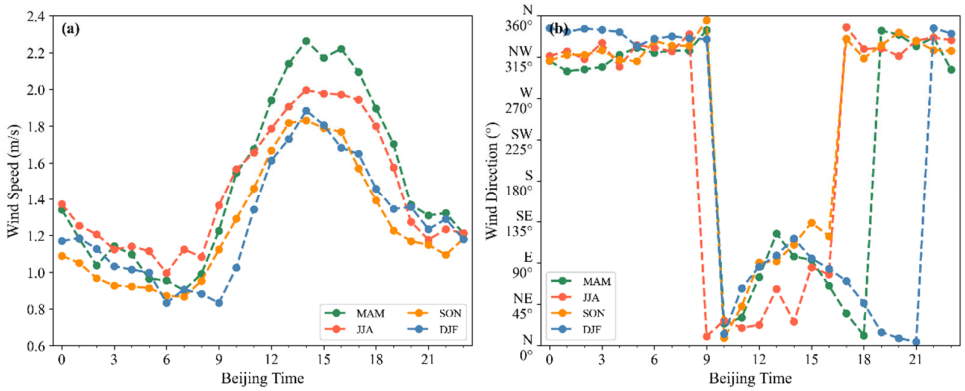

Figure 6. Diurnal variations of surface **(a)** wind speed and **(b)** wind direction across the four seasons.

The diurnal variation of vertical wind profiles within the planetary boundary layer is closely related to the dynamic and thermodynamic processes driven by the diurnal cycle of solar heating and longwave radiative cooling. Given that westerly winds prevail above 6 km, the analysis focuses on the diurnal variation and vertical distribution characteristics of the horizontal wind field within the altitude range of 0-6 km across different seasons (Figure 7). The horizontal wind field exhibits pronounced seasonal differences and diurnal variation characteristics. Driven by the mountain-valley breeze circulation, the wind field within the atmospheric boundary layer (below 1 km) in the Chengdu region shows clear diurnal variations: easterly winds (valley breeze) dominate during the daytime afternoon (12:00–17:00), shifting to northerly winds (mountain breeze) at night, with daytime wind speeds significantly lower than nighttime wind speeds. The intensity of the mountain-valley breeze circulation decreases with height. The wind field at altitudes of 1-2 km exhibits seasonal differences influenced by upper-level westerly winds. In spring and summer, easterly winds dominate throughout the day; in autumn, northeasterly winds dominate throughout the day, with westerly winds occurring during part of the daytime; in winter, westerly winds dominate near 1.5 km altitude during the daytime (08:00-16:00), shifting to northerly winds at night. With increasing altitude, the prevailing wind direction gradually transitions to westerly in all seasons. Overall, the near-surface layer is influenced by the mountain-valley breeze circulation, and

 doi:10.20944/preprints202604.1861.v1

this influence weakens with increasing altitude, while the influence of the westerly belt gradually strengthens, with the most significant influence of upper-level westerly winds occurring in winter.

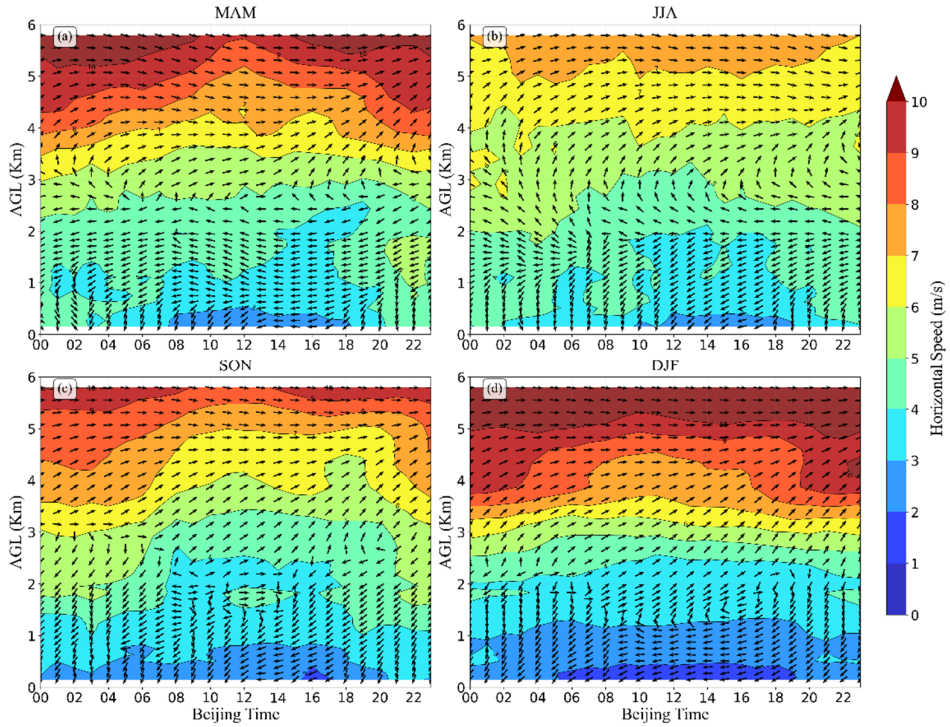

Figure 7. Diurnal variations of horizontal wind direction and speed in the middle and lower troposphere across seasons.

The upper-level wind field in each season exhibits a pronounced vertical gradient. Influenced by surface roughness, the near-surface horizontal wind speed is the lowest, and wind speed increases significantly with height. In winter, due to stable atmospheric stratification, the average daily wind speed below 1 km is low (<3 m/s), which is unfavorable for the dispersion of surface pollutants and prone to the formation of heavy pollution episodes. The horizontal wind speed at upper levels in each season exhibits typical diurnal variation characteristics, opposite to the pattern observed near the surface: the trough occurs during the daytime afternoon, while the peak occurs at night. This phenomenon may be attributed to stronger turbulent activity during the day (especially in the afternoon), while the more stable atmospheric stratification and weaker turbulence at night lead to reduced wind energy dissipation, thereby resulting in higher nighttime wind speeds compared to daytime [25].

3.4. Analysis of LLJ Characteristics

Figure 8 shows the monthly variation in the occurrence frequency of four types of LLJs, where the monthly occurrence frequency is defined as the number of hours in a given month that meet the criteria for a specific type of LLJ divided by the total number of valid observation hours in that month. In terms of monthly distribution, the peak frequency for all four LLJ types occurs in July (26.3%, 19.3%, 9.8%, and 2.7% for LLJ-1 to LLJ-4, respectively), followed by April (17.8%, 10.8%, 3.5%, and 1%, respectively). From a seasonal perspective, the occurrence frequency of the four LLJ types is highest in summer (14.2%, 9.4%, 4.1%, and 1.3% for LLJ-1 to LLJ-4, respectively), followed by spring (13.2%, 7.6%, 2.3%, and 0.7%) and autumn (10.8%, 5.4%, 1.4%, and 0.4%), and lowest in winter (5.8%, 2.6%, 0.7%, and 0). Compared with findings from other cities, the frequency of LLJs in Hefei is highest in spring, followed by summer and autumn, and lowest in winter [25]; in Beijing, LLJs occur more frequently in winter and spring, and are rare in summer [40].

 doi:10.20944/preprints202604.1861.v1

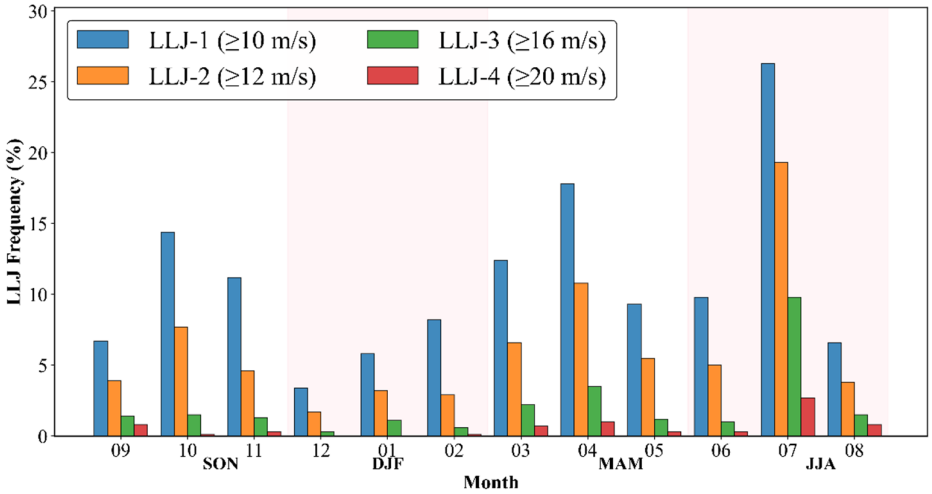

Figure 8. Monthly occurrence frequency of the four types of LLJs.

To further analyze the characteristics of LLJs, the occurrence frequencies of jet core wind speed, wind shear (defined as the wind speed difference between the surface and the jet height divided by the jet height), wind direction (corresponding to the direction of the maximum wind speed), and jet height were calculated (Figure 9), where the normalized frequency is defined as the ratio of the occurrence frequency of a specific jet feature to the total frequency of jet events. The statistical results indicate that the average wind speed of LLJs in Chengdu is 15.1 m/s, with the majority of wind speeds below 18 m/s, accounting for 78.2% (Figure 9a). The proportion of strong LLJ-4 events is 4.5%, which is higher than those observed in Tianjin (3.6%) and Shanghai (2.7%) [39].

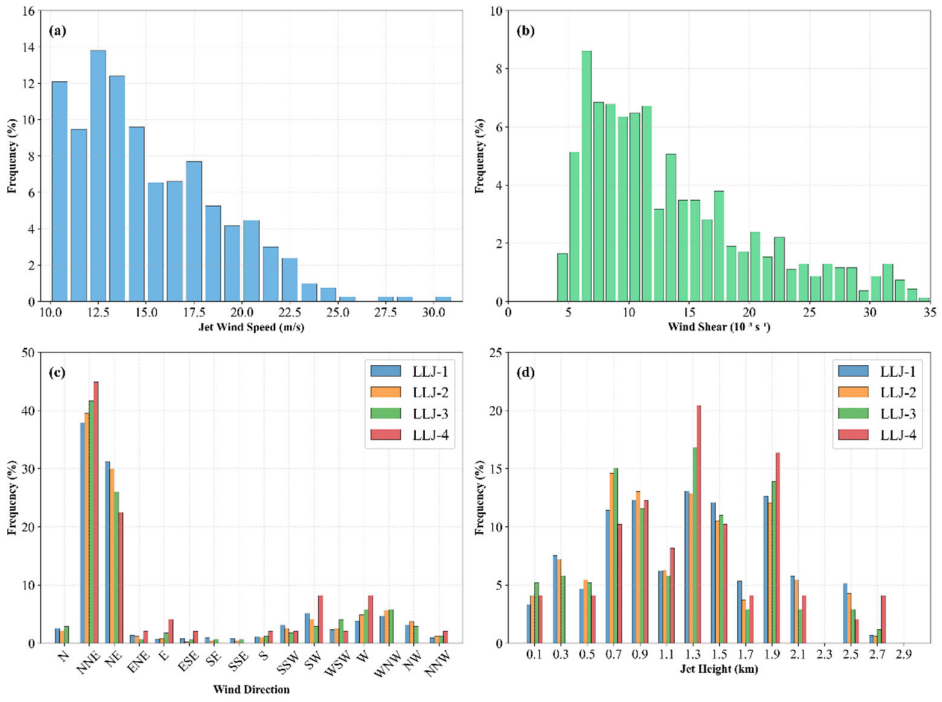

Figure 9. Frequency distribution of **(a)** wind speed, **(b)** wind shear, **(c)** wind direction, and **(d)** height of LLJs.

The average wind shear of LLJs is 0.02 s^{-1} (Figure 9b). For the four types of LLJs (LLJ-1 to LLJ-4) in Chengdu, the prevailing wind direction is north-northeasterly, followed by northeasterly (Figure 9c). The jet heights of the four LLJ types are mainly distributed between 0.7 and 1.9 km (Figure 9d), with the highest proportion for strong jets (LLJ-3 and LLJ-4) occurring at 1.3 km. Compared with

 doi:10.20944/preprints202604.1861.v1

those in Shanghai and Hefei, the LLJ heights in Chengdu are higher and more dispersed. In Shanghai, LLJ heights are concentrated within a stable layer (56.3% occur below 0.6 km) [39], while in Hefei, the annual LLJ heights range between 0.5 and 0.6 km [25].

Figure 10 shows the wind field characteristics at the LLJs nose height across different seasons. In winter and spring, the dominant wind direction of LLJs is northeast, while in summer and autumn it is north-northeast, with the wind direction being more concentrated in summer and winter. Analysis combined with Figure 5 reveals that the wind direction distribution of LLJs in Chengdu is significantly influenced by the background wind field.

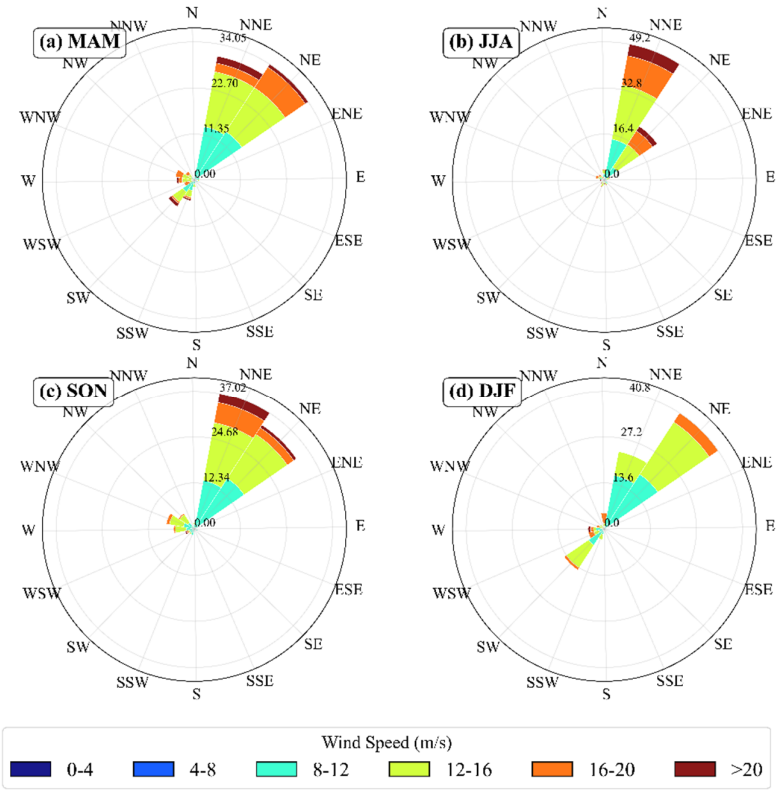

Figure 10. Seasonal wind rose diagrams of LLJs at nose height.

The diurnal variation in the formation and occurrence of LLJs is influenced by the interaction between surface heating/cooling cycles, atmospheric stability, and synoptic-scale weather patterns [25]. Due to the association between jets and boundary layer evolution, the occurrence frequency of LLJs displays a clear diurnal pattern. For LLJ-1 to LLJ-4, the occurrence frequencies during the daytime were 46, 23, 6, and 4 times, respectively, while those at night were 93, 52, 21, and 5 times, respectively (Figure 11a), indicating that the frequency of LLJs is significantly higher at night than during the daytime. According to the classical theoretical description of inertial oscillations, nocturnal LLJs (NLLJs) form due to the decoupling of nocturnal winds from surface friction, facilitated by the development of a near-surface temperature inversion [22]. The nocturnal temperature inversion effectively reduces the influence of surface friction on the air above it [52]. The peak frequencies for all four jet types occur at night, with those of LLJ-1 and LLJ-2 peaking at 22:00, and those of LLJ-3 and LLJ-4 at 21:00. Although the occurrence frequency of jets is lower during the daytime due to strong turbulent mixing, a considerable number of jets are still observed in the daytime boundary layer. The persistence of these daytime jets is related to boundary layer stability, if the mixed layer develops weakly after sunrise and turbulent mixing is insufficient to completely disrupt the nighttime jet structure, high wind speed features can persist [39]. A typical LLJ event was selected to analyze the average wind speed profiles at different hours (Figure 11b) in order to further understand the development characteristics of LLJs. This LLJ event occurred from 05:00 on July 8,

 doi:10.20944/preprints202604.1861.v1

2024, to 18:00 on July 10, 2024, lasting a total of 62 hours. The results show that the jet intensity gradually increased after sunset, with the average wind speed profile peaking at 02:00 (18.4 m/s) before gradually decreasing, and the jet core height was mostly concentrated below 1.4 km. The jet intensity was significantly higher at night than during the daytime.

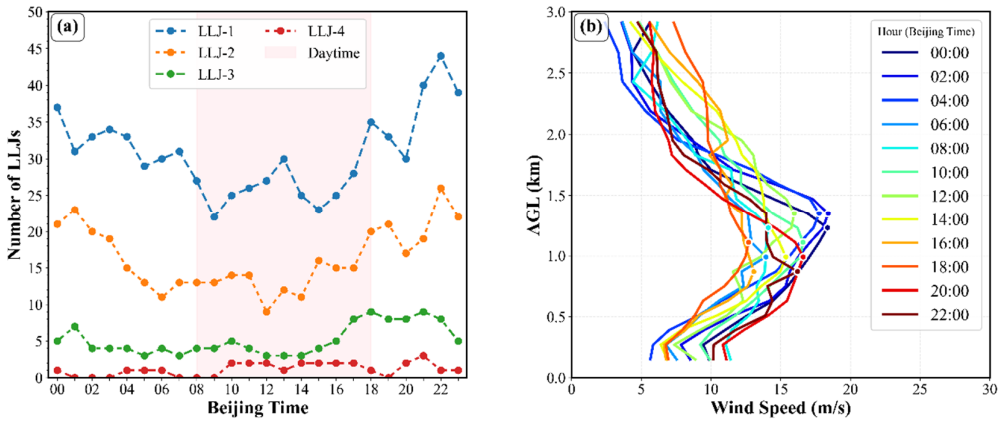

Figure 11. (a) Diurnal variation of occurrence frequency for four types of LLJs (Pink shading indicates daytime), and **(b)** average wind speed profiles at different times for a typical LLJ event.

4. Discussion

This study leverages the high spatiotemporal resolution of RWP to characterize in detail the vertical distribution and evolution characteristics of the wind field and LLJs in the middle and lower troposphere over Chengdu. On the application front, the findings contribute to the precise early warning of severe weather events such as heavy rainfall, the scientific management of air pollution control, and the support of safe operation assurance for the low-altitude economy. Despite these insights, this study is limited to a single urban observation site and focuses on statistical analysis. Future research will expand observations to multiple sites to comprehensively capture the spatial variability of LLJ characteristics over complex terrain. Furthermore, subsequent studies will conduct specific case analyses under different meteorological scenarios, aiming to deepen our theoretical understanding of the complex feedback processes between the boundary layer and weather systems.

5. Conclusions

This study utilized one year of tropospheric RWP observations to systematically describe the vertical distribution and evolution characteristics of the wind field and LLJs in the middle and lower troposphere over the Chengdu region, through an analysis of their seasonal and diurnal variations. The main conclusions are as follows:

(1) The effective detection height of the RWP reaches 7.4 km throughout the year. The monthly data acquisition rate is highest in October (98.7%) and lowest in August (90.1%). Compared with radiosonde data, the RWP shows better consistency in summer and autumn. Despite seasonal differences, the horizontal wind speeds from the RWP and radiosonde data exhibit good consistency in the middle and lower troposphere (0-6 km) throughout the year.

(2) The mean wind speed of the entire atmospheric layer is highest in winter, followed by spring and autumn, and lowest in summer. The mean wind speed in all four seasons increases with height, with the highest vertical gradient occurring in winter. In the lower troposphere (0-2 km), the prevailing wind directions are north-northeasterly and northeasterly; in the middle layer (2-5 km), southerly and southwesterly winds dominate; and in the upper layer (5-8 km), westerly winds prevail. Horizontal wind speed increases slowly with height below 3 km and accelerates significantly above 3 km.

 doi:10.20944/preprints202604.1861.v1

(3) The wind field in the middle and lower troposphere exhibits pronounced diurnal and seasonal variations. Within the atmospheric boundary layer (below 1 km), the wind field shows a distinct diurnal variation: easterly winds dominate during the daytime afternoon (12:00–17:00), shifting to northerly winds at night. The peak surface wind speed occurs in the afternoon, while the peak upper-level wind speed occurs at night. The prevailing wind direction in the lower layer is mainly influenced by mountain-valley breezes, with increasing altitude, the westerly belt gradually becomes the dominant wind system, with the most significant influence of the westerly belt occurring in winter.

(4) The occurrence frequency of LLJs is highest in July, followed by April. From a seasonal perspective, the occurrence frequency of LLJs is highest in summer, followed by spring and autumn, and lowest in winter. The wind speeds of LLJs are mostly below 18 m/s. The dominant wind direction of LLJs is northeast in spring and winter, and north-northeast in summer and autumn. The jet height distribution is relatively dispersed, mainly ranging from 0.7 to 1.9 km. Both the frequency and intensity of LLJs exhibit clear diurnal variations, with higher values at night than during the day.

Author Contributions: Conceptualization, T.D.; methodology, T.D. and C.W.; software, T.D. and C.W.; validation, T.D.; formal analysis, T.D. and X.H.; investigation, T.D., X.H. and P.T.; resources, T.D.; data curation, T.D. and Y.S.; writing—original draft preparation, T.D.; writing—review and editing, P.T., Y.R. and J.D.; visualization, T.D. and C.W.; supervision, T.D.; project administration, T.D.; funding acquisition, T.D. All authors have read and agreed to the published version of the manuscript.

Funding: This research was supported by the National Key Research and Development Program of China (grant no. 2023YFC3007501), the Heavy Rain and Drought-Flood Disasters in Plateau and Basin Key Laboratory of Sichuan Province (SCQXKJQN202416), the National Natural Science Foundation of China under grant number 42405075, and the Natural Science Foundation of Chongqing under grant number CSTB2024NSCQ-MSX0612.

Data Availability Statement: The data used in this study are available upon request from the corresponding author due to privacy restrictions.

Acknowledgments: The authors thank the Chengdu Meteorological Bureau for their support with observational data. During the preparation of this manuscript, the authors used DeepSeek for the purposes of English language polishing and translation. The authors have reviewed and edited the output and take full responsibility for the content of this publication.

Conflicts of Interest: The authors declare no conflicts of interest.

Abbreviations

The following abbreviations are used in this manuscript:

LLJ	Low-Level Jet
RWP	Wind Profiler Radar
DAR	Data Acquisition Rate
AGL	Above the Ground Level
HWS	Horizontal Wind Speed
HWD	Horizontal Wind Direction
VWS	Vertical Wind Speed

 doi:10.20944/preprints202604.1861.v1

References

1. Liu, B.; Guo, J.; Gong, W.; Shi, Y.; Jin, S. Boundary layer height as estimated from Radar wind profilers in four cities in China: Relative contributions from aerosols and surface features. Remote Sensing 2020, 12, 1657.
2. Guo, J.; Liu, B.; Gong, W.; Shi, L.; Zhang, Y.; Ma, Y.; Zhang, J.; Chen, T.; Bai, K.; Stoffelen, A. First comparison of wind observations from ESA's satellite mission Aeolus and ground-based radar wind profiler network of China. Atmospheric Chemistry and Physics 2021, 21, 2945-2958.
3. Huang, J.; Ma, J.; Guan, X.; Li, Y.; He, Y. Progress in semi-arid climate change studies in China. Advances in Atmospheric Sciences 2019, 36, 922-937.
4. Huang, X.; Ding, A.; Gao, J.; Zheng, B.; Zhou, D.; Qi, X.; Tang, R.; Wang, J.; Ren, C.; Nie, W. Enhanced secondary pollution offset reduction of primary emissions during COVID-19 lockdown in China. National science review 2021, 8, nwaa137.
5. Stettner, D.; Velden, C.; Rabin, R.; Wanzong, S.; Daniels, J.; Bresky, W. Development of enhanced vortex-scale atmospheric motion vectors for hurricane applications. Remote Sensing 2019, 11, 1981.
6. Yang, Y.; Fan, S.; Wang, L.; Gao, Z.; Zhang, Y.; Zou, H.; Miao, S.; Li, Y.; Huang, M.; Yim, S.H.L. Diurnal evolution of the wintertime boundary layer in urban Beijing, China: Insights from Doppler Lidar and a 325-m meteorological tower. Remote Sensing 2020, 12, 3935.
7. Wei, W.; Zhang, H.; Zhang, X.; Che, H. Low-level jets and their implications on air pollution: A review. Frontiers in Environmental Science 2023, 10, 1082623.
8. Smith, E.N.; Gebauer, J.G.; Klein, P.M.; Fedorovich, E.; Gibbs, J.A. The Great Plains low-level jet during PECAN: Observed and simulated characteristics. Monthly Weather Review 2019, 147, 1845-1869.
9. King, J.A.; Engelstaedter, S.; Washington, R.; Munday, C. Variability of the Turkana low-level jet in reanalysis and models: Implications for rainfall. Journal of Geophysical Research: Atmospheres 2021, 126, e2020JD034154.
10. Sánchez, M.P.; Pereira de Oliveira, A.; Varona, R.P.; Tito, J.V.; Codato, G.; Ynoue, R.Y.; Ribeiro, F.N.D.; Marques Filho, E.P.; da Silveira, L.C. Observational Investigation of the Low-Level Jets in the Metropolitan Region of São Paulo, Brazil. Earth and Space Science 2022, 9, e2021EA002190.
11. Ma, X.; Li, Y.; Li, Z.; Huo, F. Investigation of the characteristics of low-level jets over North America in a convection-permitting Weather Research and Forecasting simulation. Atmospheric Chemistry and Physics 2024, 24, 12013-12030.
12. Bonner, W.D. Climatology of the low level jet. Monthly Weather Review 1968, 96, 833-850.
13. Ding, J.; Ren, Y.; Zhang, H.; Chang, H.; Hu, Z.; Liang, J.; Zhang, K.; Wang, S.; Cao, X.; Tian, P. Mechanism of turbulence structure evolution in the nocturnal boundary layer during the interaction of low-level jet and internal gravity waves: Based on full boundary layer turbulence observations. Journal of Geophysical Research: Atmospheres 2025, 130, e2024JD042106.
14. Du, Y.; Chen, G. Climatology of low-level jets and their impact on rainfall over southern China during the early-summer rainy season. Journal of Climate 2019, 32, 8813-8833.
15. Wei, W.; Zhang, H.; Wu, B.; Huang, Y.; Cai, X.; Song, Y.; Li, J. Intermittent turbulence contributes to vertical dispersion of PM 2.5 in the North China Plain: cases from Tianjin. Atmospheric Chemistry and Physics 2018, 18, 12953-12967.
16. Hu, X.-M.; Klein, P.M.; Xue, M.; Zhang, F.; Doughty, D.C.; Forkel, R.; Joseph, E.; Fuentes, J.D. Impact of the vertical mixing induced by low-level jets on boundary layer ozone concentration. Atmospheric Environment 2013, 70, 123-130.
17. Céspedes, J.; Kotthaus, S.; Preissler, J.; Toupoint, C.; Thobois, L.; Drouin, M.-A.; Dupont, J.-C.; Faucheux, A.; Haeffelin, M. The Paris low-level jet during PANAME 2022 and its impact on the summertime urban heat island. Atmospheric Chemistry and Physics 2024, 24, 11477-11496.
18. Zhang, X.; Luo, Y.; Du, Y. Observation of boundary-layer jets in the northern South China Sea by a research vessel. Remote Sensing 2024, 16, 3872.
19. Han, Z.; Ge, J.; Chen, X.; Hu, X.; Yang, X.; Du, J. Dust activities induced by nocturnal low-level jet over the Taklimakan desert from WRF-Chem simulation. Journal of Geophysical Research: Atmospheres 2022, 127, e2021JD036114.

 doi:10.20944/preprints202604.1861.v1

20. Lin, Y.; Wang, C.; Yan, J.; Li, J.; He, S. Observation and simulation of low-level jet impacts on 3D urban heat islands in Beijing: A case study. Journal of the Atmospheric Sciences 2022, 79, 2059-2073.
21. Chen, Y.; Tu, C.; Hsiao, F.; Chen, C.; Lin, P.; Lin, P. An overview of low-level jets (LLJs) and their roles in heavy rainfall over the Taiwan area during the early summer rainy season. Meteorology, 1, 64–112. 2022.
22. Blackadar, A.K. Boundary layer wind maxima and their significance for the growth of nocturnal inversions. Bulletin of the American Meteorological Society 1957, 38, 283-290.
23. Zheng, J.; Liu, Y.; Peng, T.; Wan, X.; Huang, X.; Wang, Y.; Che, Y.; Xu, D. Investigating wind characteristics and temporal variations in the lower troposphere over the northeastern Qinghai–Tibet Plateau using a Doppler LiDAR. Remote Sensing 2024, 16, 1840.
24. Zong, L.; Yang, Y.; Xia, H.; Yuan, J.; Guo, M. Elucidating the impacts of various atmospheric ventilation conditions on local and transboundary ozone pollution patterns: a case study of Beijing, China. Journal of Geophysical Research: Atmospheres 2023, 128, e2023JD039141.
25. Wei, T.; Wang, M.; Wu, K.; Yuan, J.; Xia, H.; Lolli, S. Characterizing urban planetary boundary layer dynamics using 3-year Doppler wind lidar measurements in a western Yangtze River Delta city, China. Atmospheric Measurement Techniques 2025, 18, 1841-1857.
26. Zhou, X.; Zhang, C.; Li, Y.; Chen, Z.; Zhang, J.; Ding, X. Wind gust parameters in the lower troposphere based on Doppler Lidar data. Journal of Geophysical Research: Atmospheres 2023, 128, e2022JD038156.
27. Rubio, H.; Kühn, M.; Gottschall, J. Evaluation of low-level jets in the southern Baltic Sea: a comparison between ship-based lidar observational data and numerical models. Wind Energy Science Discussions 2022, 2022, 1-29.
28. Li, X.; Du, Y. Statistical relationships between two types of heavy rainfall and low-level jets in South China. Journal of Climate 2021, 34, 8549-8566.
29. Sun, X.; Zhou, Y.; Zhao, T.; Bai, Y.; Huo, T.; Leng, L.; He, H.; Sun, J. Effect of vertical wind shear on PM2. 5 changes over a receptor region in Central China. Remote Sensing 2022, 14, 3333.
30. Yan, Y.; Cai, X.; Wang, X.; Miao, Y.; Song, Y. Low-level jet climatology of China derived from long-term radiosonde observations. Journal of Geophysical Research: Atmospheres 2021, 126, e2021JD035323.
31. Dolman, B.K.; Reid, I.M.; Tingwell, C. Stratospheric tropospheric wind profiling radars in the Australian network. Earth, Planets and Space 2018, 70, 170.
32. Liu, B.; Ma, Y.; Guo, J.; Gong, W.; Zhang, Y.; Mao, F.; Li, J.; Guo, X.; Shi, Y. Boundary layer heights as derived from ground-based radar wind profiler in Beijing. IEEE Transactions on Geoscience and Remote Sensing 2019, 57, 8095-8104.
33. Ishihara, M.; Kato, Y.; Abo, T.; Kobayashi, K.; Izumikawa, Y. Characteristics and performance of the operational wind profiler network of the Japan Meteorological Agency. Journal of the Meteorological Society of Japan. Ser. II 2006, 84, 1085-1096.
34. Liu, B.; Guo, J.; Gong, W.; Shi, L.; Zhang, Y.; Ma, Y. Characteristics and performance of wind profiles as observed by the radar wind profiler network of China. Atmospheric Measurement Techniques 2020, 13, 4589-4600.
35. Wei, W.; Wu, B.; Ye, X.; Wang, H.; Zhang, H. Characteristics and mechanisms of low-level jets in the Yangtze River Delta of China. Boundary-Layer Meteorology 2013, 149, 403-424.
36. Deng, X.; He, D.; Zhang, G.; Zhu, S.; Dai, R.; Jin, X.; Fu, W.; Shen, W.; Chen, J.; Fan, Y. Comparison of horizontal wind observed by wind profiler radars with ERA5 reanalysis data in Anhui, China. Theoretical and Applied Climatology 2022, 150, 1745-1760.
37. Solanki, R.; Guo, J.; Lv, Y.; Zhang, J.; Wu, J.; Tong, B.; Li, J. Elucidating the atmospheric boundary layer turbulence by combining UHF radar wind profiler and radiosonde measurements over urban area of Beijing. Urban Climate 2022, 43, 101151.
38. Li, N.; Guo, J.; Wu, M.; Zhang, F.; Guo, X.; Sun, Y.; Zhang, Z.; Liang, H.; Chen, T. Low-level jet and its effect on the onset of summertime nocturnal rainfall in Beijing. Geophysical Research Letters 2024, 51, e2024GL110840.
39. Wei, W.; Zhang, H.; Ye, X. Comparison of low-level jets along the north coast of China in summer. Journal of Geophysical Research: Atmospheres 2014, 119, 9692-9706.

 doi:10.20944/preprints202604.1861.v1

40. Miao, Y.; Guo, J.; Liu, S.; Wei, W.; Zhang, G.; Lin, Y.; Zhai, P. The climatology of low-level jet in Beijing and Guangzhou, China. Journal of Geophysical Research: Atmospheres 2018, 123, 2816-2830.
41. YANG, K.; GAO , Z.; GAO, B.; Xiao, T.; YANG, G. Spatiotemporal Distribution Characteristics Research of Wind Field and Wind Shear on the East Coast of Erhai Lake in the Southeast Edge of Hengduan Mountain Area. Plateau Meteorology 2025, 44, 462-474.
42. Li, N.; Guo, J.; Guo, X.; Chen, T.; Zhang, Z.; Tang, N.; Wang, Y.; Yang, H.; Zheng, Y.; Zhou, Y. On the nationwide variability of low-level jets prior to warm-season nocturnal rainfall in China revealed by radar wind profilers. Atmospheric Chemistry and Physics 2026, 26, 3339–3356.
43. WANG, J.; ZHANG, Q.; ZHANG, T.; LONG, K.; SHI, R. Low—level Wind Field Characteristic Observed by Wind Profile Radar During Two Rainstorm Processes in Chengdu. Journal of Arid Meteorology 2021, 39, 87-95.
44. Zhang, H.; Zhou, Y.; Lai, Z.; Deng, G. Overshooting convection and torrential precipitation associated with the mesoscale northerly low-level jets in the Sichuan Basin, China. Atmospheric Research 2024, 310, 107604.
45. HU, D.; XIE, X.; CHEN, C.; Zhou, Q. Wind Field Characteristics of Heavy Precipitation Process in Western Sichuan Basin Based on Wind Profiler Radar Data. Plateau Meteorology 2025, 44, 240-252.
46. Xiong, J.; Li, J.; Gao, F.; Zhang, Y. City wind impact on air pollution control for urban planning with different time-scale considerations: A case study in Chengdu, China. Atmosphere 2023, 14, 1068.
47. Lei, Y.; Wu, K.; Zhang, X.; Kang, P.; Du, Y.; Yang, F.; Fan, J.; Hou, J. Role of meteorology-driven regional transport on O3 pollution over the Chengdu Plain, southwestern China. Atmospheric Research 2023, 285, 106619.
48. Cao, Y.; Zhao, X.; Su, D.; Cheng, X. Analysis of Regional Differences in Boundary Layer Horizontal Wind Fields in the Transition Zone Between Mountains and Plains in Western Chengdu. METEOROLOGICAL SCIENCE AND TECHNOLOGY 2024, 52, 743-752.
49. Zhu, L. Preliminary Quality Analysis of Horizontal Wind Products from Wind Profiler Radar for Data Assimilation. METOROLOGICA MONTHLY 2015, 41, 1494-1502.
50. WANG, Y.; ZHANG, W.; ZHAO, Y. Analysis of Wind Characteristics of Wind-Profiler Radars and Their Quality Control Methods for Data Assimilation. Chinese Journal of Atmospheric Sciences 2021, 45, 123–147.
51. Yao , H.; Li , D. Spatial structure of East Asia subtropical jet stream and its relation with winter air temperature in China. Chinese Journal of Atmospheric Sciences (in Chinese) 2013, 37, 881–890.
52. Mirza, A.K.; Dacre, H.F.; Lo, C.H.B. A case study analysis of the impact of a new free tropospheric turbulence scheme on the dispersion of an atmospheric tracer. Quarterly Journal of the Royal Meteorological Society 2024, 150, 1907-1925.